JTTEE5 18:835–845
DOI: 10.1007/s11666-009-9389-z
1059-9630/$19.00 © ASM International

Lifetime of Plasma-Sprayed Thermal Barrier Coatings: Comparison of Numerical and Experimental Results

Robert Vaßen, Stephan Giesen, and Detlev Stöver

(Submitted February 22, 2009; in revised form August 20, 2009)

Atmospherically sprayed thermal barrier coatings (TBCs) are nowadays an essential part in modern gas turbines. However, a design integrated use of these coatings is only possible with reliable lifetime models. In this paper, a model is outlined which describes the major failure in TBCs associated with the growth of a thermally grown oxide (TGO) on the bond coat (BC). An essential part of the model is a simplified description of the crack growth as a result of thermal cycling and TGO growth. In addition, the energy release rate for the system is calculated and compared to an estimated critical energy release rate reduced by the crack growth. If both are equal, failure is assumed. The results of the modeling are compared to thermal cycling experiments partly applying a thermal gradient. BC temperatures and also microstructures of the ceramic topcoat have been varied and the influence on the cyclic life studied.

Keywords coatings for engine components, high-temperature oxidation, property of coatings, TBC topcoats, thermal cycling

1. Introduction

Thermal barrier coatings (TBCs) are in use in gas turbines since more than three decades. However, still these coatings are not fully integrated in the design as a failure between two service intervals and a subsequent harsh damage of the gas turbine cannot be totally excluded. To overcome this situation, reliable lifetime prediction in combination with good reproducibility of the coatings is an important research target. In the past, many efforts have been made to calculate the stress levels in TBCs, especially by finite element (FE) methods (Ref 1-6). These models have to include the complex microstructure at the interface between TBC and topcoat. In APS TBCs, this interface is not flat as typically found in the electron beam physical vapor deposition (EB-PVD) type coatings. Instead a rough interface with roughness values well above 6 μm is used. This rather high roughness values are essential for a sufficient bonding between topcoat and bond coat (BC). On the other hand, they introduce additional stress levels in the ceramic coating due to the curvature. Depending on the type of curvature, both tensile or compressive stress levels can be generated within the TBC and also in the TGO. This fact was already pointed out by Chang and Pucharoen 20 years ago (Ref 7). Many detailed calculations have been performed and different possible crack paths have been suggested. However, still it is difficult to transfer these complex results to a more general description of the lifetime. Instead, more generalized approaches have been used. An early attempt was made by Miller and within a NASA project (Ref 8, 9), in which the number of cycles to failure N is a function of the strain range $\Delta\varepsilon$ and a critical strain range $\Delta\varepsilon_c$, which is a function of the ratio of TGO thickness δ and the critical TGO thickness δ_c:

$$N = \left(\frac{\Delta\varepsilon_c(\delta/\delta_c)}{\Delta\varepsilon}\right)^a \quad \text{(Eq 1)}$$

Oechsner described a lifetime prediction approach for TBC systems in which critical energy release rates are compared to the actual energy release rate in the system (Ref 10). Microstructural changes in the system lead to a reduction of the first, while the second is increasing. Failure occurs when both values are equal.

Renusch et al. (Ref 11, 12) developed a model based on the evaluation of strains in the coating system which are partly extracted from experimental data.

Beck et al. presented a phenomenological lifetime prediction model in which first an incubation period is assumed (Ref 13, 14). This period ends when a certain TGO thickness is reached. In the second phase, crack growth is governed by a fracture mechanics approach.

Busso et al. (Ref 15) presented a software tool in which thermo-elastic and visco-plastic effects are considered to evaluate stress levels with a FE code. These stress values are compared with a failure stress extracted from experimental data.

In the present approach, it is assumed that the cracks mainly propagate within the topcoat close to the TGO. An incubation period for the cracks is not necessary as microstructural investigations show that many

Robert Vaßen, Stephan Giesen, and **Detlev Stöver**, IEF-1, Forschungszentrum Jülich GmbH, Jülich, Germany. Contact e-mail: r.vassen@fz-juelich.de.

microcracks with crack lengths above 50 μm are present in the as-sprayed condition (Ref 5). The crack growth reduces the bonding area between topcoat and substrate/BC and by that the critical energy release rate. The energy release rate is calculated by cooling a stress-free system from elevated temperature to room temperature. If energy release rate and critical energy release rate are equal, failure is assumed similar to the model described by Oechsner (Ref 10). Certainly, several simplifications are made in the model, however, the model is based on microstructural considerations and all parameters can be interpreted in terms of such properties. In fact, different microstructural features of the ceramic topcoat of the TBC system can be described by model parameters. Having this capability, the model allows the evaluation of the influence of coating microstructure on the lifetime and furthermore, suggestions should be possible for a further optimization of the ceramic topcoat.

2. Model Description

Parts of the model have been described in earlier publications (Ref 6, 16, 17) and will therefore be outlined here only shortly. The basic idea of the model is the growth of pre-existing cracks in the APS TBC close to the BC due to the stress state generated during the thermal cycling. That this type of crack growth really exists in thermally cycled TBCs was already shown in Ref 5, a recompilation of the data is presented in Fig. 1. The calculation of the stress level is made in a simplified way, which is made on purpose to keep the number of parameters rather small. Assuming a stress-free state for the as-sprayed conditions, in-plane tensile stresses are generated during the high-temperature phase within the TBC due to the higher thermal expansion coefficient of the substrate compared to the coating. We assume here that this stress level relax rather fast due high creep rates within the ceramics and the BCs. For our coatings, viscosity and Young's modulus data of about 10 GPa h and 20 GPa have been determined at 1000 °C (Ref 18), which indicate a stress relaxation even at 1000 °C within hours. Assuming a stress-free high-temperature state also avoids the need of time-consuming FE calculations for a large number of thermal cycles.

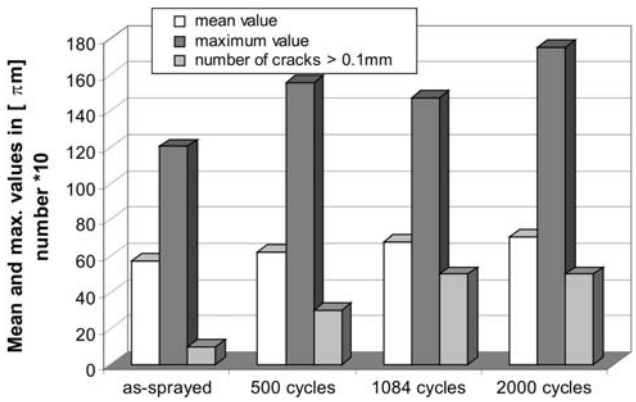

Fig. 1 Evolution of the mean crack size, the maximum crack length and the number of cracks larger than 100 μm at the center of a thermally cycled TBC system, BC and surface temperature 1000, and 1250 °C, respectively, heating time 5 min (about 4 min at temperature), cooling time 2 min (Ref 20)

During cooling, compressive in-plane stresses are generated within the TBC. Within the presented approach, these stress levels are calculated using FE programmes (ANSYS) assuming linear elastic behavior without creep or plasticity. As discussed, creep or plasticity is implicitly introduced by using a stress-free state at operation temperature. The model also automatically indicates that the influence of heating and cooling rates is only given by modifying times at temperature and not by relaxation of stress states during the transients. A key feature of our model is the assumption of a rough interface between BC and TBC. This rough interface is essential for a good performance of the system as it gives the good mechanical interlocking of ceramic topcoat and metallic parts. Typical roughness values are between 6 and 12 μm. Due to the curvature of these rough interfaces, additional stress levels are generated which have been pointed out earlier (Ref 7). At first, tensile stresses are found at hill locations in the TBC, here the cracks can grow till they reach the valley locations, where compressive stress levels are found (see Fig. 2a). Further crack extension is only possible after the growth of a sufficiently large TGO layer which leads to a stress inversion (Fig. 2b). In our calculations, the rough surface was approximated by a sinusoidal function with a wavelength L and an amplitude A. At the valley location, the stress values in a perpendicular direction to the interface as a result of the FE calculations have then been fitted by an analytical formula based on analytical considerations:

$$\sigma_{yy,\mathrm{valley}}(y) \approx \bar{\alpha} E_{\mathrm{TBC}} (\alpha_{\mathrm{BC}} - \alpha_{\mathrm{TBC}}) |\Delta T| \frac{A}{L} \exp\left(-\frac{2\pi}{L} y\right) \times \left[\left(1 + \frac{2\pi}{L} y\right) - \bar{\beta} \frac{\alpha_{\mathrm{BC}} - \alpha_{\mathrm{TGO}}}{\alpha_{\mathrm{BC}} - \alpha_{\mathrm{TBC}}} \frac{d_{\mathrm{TGO}}}{A} \times \left(1 + \bar{\gamma} \frac{A}{d_{\mathrm{TGO}}} \exp\left(-\bar{\delta} \frac{A}{d_{\mathrm{TGO}}}\right) \frac{2\pi}{L} y\right)\right] \quad \text{(Eq 2)}$$

in which $\bar{\alpha}$, $\bar{\beta}$, $\bar{\gamma}$, $\bar{\delta}$ are fitting constants of the order of ± 1, α_i the thermal expansion coefficients of BC, TBC, or TGO, E_{TBC} Young's modulus of the TBC, ΔT the temperature drop during cooling at the interface, d_{TGO} the TGO thickness, and y the distance perpendicular from the interface TBC/TGO within the TBC. The first exponential factor will lead to a fast reduction of the stress state within the coating for larger values of y/L.

The fit was based on different calculations: at a constant wavelength of 70 μm with amplitudes of 5, 10, and 15 μm, and at constant amplitude of 10 μm with wavelengths of 40, 70, and 100 μm. For each calculation, the TGO thickness of 0, 4, 8, and 12 μm was taken.

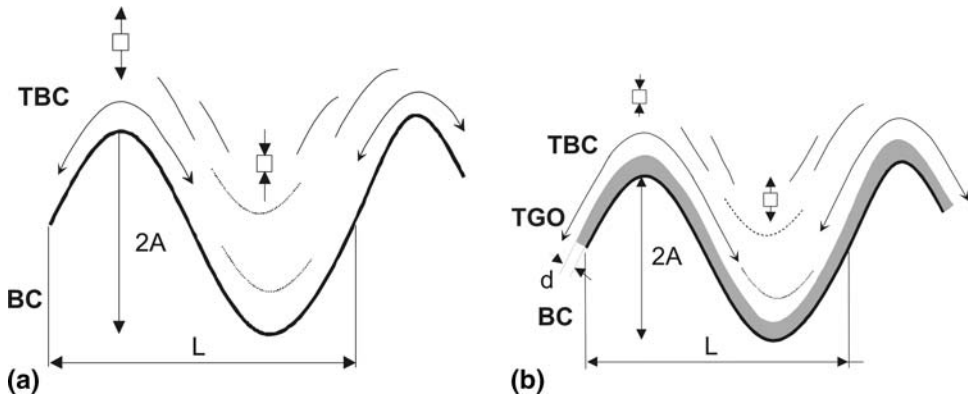

Fig. 2 Schematic of the stress levels in a TBC system: (a) as-sprayed and (b) after TGO growth

The difference between the analytical and the FE results is typically below 20%, only close to the stress inversion it is larger.

The growth of the TGO is described by a conventional growth law:

$$d_{\mathrm{TGO}} = A_{\mathrm{TGO}} \exp\left(-\frac{E_{\mathrm{TGO}}}{k_{\mathrm{B}} T}\right) t^{p} \qquad \text{(Eq 3)}$$

where A_{TGO}, E_{TGO}, and p are the parameters, and k_{B} is the Boltzman constant.

In addition, also tensile stress levels generated by a curved substrate (e.g., a cylindrical sample) are added in a similar way as described in Ref 17 giving an inverse dependence of the stress state on the radius of curvature.

These stress values are then introduced into a subcritical crack growth law (Ref 19):

$$\frac{da}{dt} = A^{*} \left(\frac{K(a,\sigma)}{K_{\mathrm{I,c}}}\right)^{m} \qquad \text{(Eq 4)}$$

in which A^* is a constant and $K(a, \sigma)$ and $K_{\mathrm{I,c}}$ are the stress and the critical stress intensity factors and m an exponent fixed to 18. With $K = Y\sigma a^{1/2}$ one can rewrite the equation to:

$$\int_{a_0}^{a_{\mathrm{f}}} \frac{da}{a^{m/2}} = \frac{A^{*} Y^{m}}{K_{\mathrm{I,c}}^{m}} \int_{t_0}^{t_{\mathrm{f}}} \sigma^{m} dt \qquad \text{(Eq 5)}$$

with the indices 0 and f indicating crack length and time at the beginning and at failure, and $A * (Y/K_{\mathrm{Ic}})^m$ being a fitting factor. We assume a starting crack length of half the wavelength of the roughness profile ($L/2$). Of course, in the given calculation of the stress intensity factor the geometrical factor is probably different for each crack geometry; however, this is ignored for simplicity.

If the stress levels in the TBC are positive (tensile) crack growth starts. The maximum length the cracks can reach is the full wavelength. In our old model at this stage, the cracks are interconnected and the coating spalls off. In our present approach, failure can take place even earlier as outlined below.

It is well-known that sintering plays a major role for the performance of TBC system. This item is introduced in the model by an increase of the Young's modulus E by the sintering:

$$E_{\mathrm{TBC}}(t) = \frac{\beta E_{\mathrm{TBC}}^{0} E_{\mathrm{TBC}}^{\infty}}{\beta E_{\mathrm{TBC}}^{0} + E_{\mathrm{TBC}}^{\infty} - E_{\mathrm{TBC}}^{0}}$$
$$\text{with} \quad \beta = 1 + A_{\mathrm{sint}} \exp\left(-\frac{E_{\mathrm{sint}}}{k_{\mathrm{B}} T}\right) t^{n} \qquad \text{(Eq 6)}$$

with 0 and ∞ indicating the starting and the bulk modulus, A_{sint}, E_{sint}, and n are parameters to describe the sintering kinetics. In contrast to our old description, this model approaches for infinite time the bulk value and not infinity which is more realistic. The increase of Young's modulus leads to an increase in the stress levels according to Eq 2.

Up to now the model does not contain factors which really describe the cyclic effect of the thermo mechanical loading. In principle, the results should be quite similar comparing the lifetime of samples cycled with short or long dwell times as long as the ratio between high and low temperature phase is similar. On the other hand, experimentally it is observed that the lifetime is reduced considerably if the cycle length is reduced (see e.g., Ref 20). A possible mechanism which can explain such effects of the cycle length is stress relaxation. It has been found that such relaxation processes can take place even at room temperature (Ref 18). A simple approach considers the stress reduction as follows:

$$\frac{d\sigma}{dt} = E\frac{d\varepsilon}{dt} = E\frac{\sigma}{\eta} \Rightarrow \sigma = \sigma_0 \exp\left(-\frac{E}{\eta} t\right) \qquad \text{(Eq 7)}$$

in which η is the viscosity and σ/σ_0 gives the stress level reduction during the time t. This function is now introduced into Eq 5. Hence, starting stress levels from Eq 2 are reduced during the crack growth at room temperature and lifetime is prolonged.

The model described so far is focused on the stress state close to the interface BC/TBC. The stress states are hardly influenced by the stress state in the ceramic far way from the interface or by the thickness of the TBC. Also here, the experience shows that the thickness plays a major role

and should be introduced. A possible way to do that is to estimate from the crack growth the reduction of the interfacial bonding and to compare this with the critical energy release rate buildup in the TBC. For the first term, it is assumed that the cracks of length a will reduce the area of the interface and hence the critical energy release rate G_{crit} reaching at infinite crack lengths a certain fraction of 10%. A simple formula giving this behavior is

$$G_{crit} = \left(a_1 - a_2\left(1 - \exp\left(-\frac{a}{L}\right)\right)^2\right) G^0_{crit} \quad \text{(Eq 8)}$$

The factors a_1 and a_2 are determined to start at the starting crack length $a_0 = L/2$ with the critical energy release rate of the as-sprayed material and giving 10% of it at infinite crack length. In Ref 10, values of 100 and 200 J/m^2 are given for the critical energy release rate, we assume a mean value of 150 J/m^2. The extension of the possible crack length beyond L avoids the introduction of a rather artificial maximum crack length. This procedure does not effect lifetime significantly as growth is very fast for crack lengths larger than L.

The energy release rate stored in the coating is approximated by an integration of the stress level across the spalling coating thickness ($d_{TBC} - y$) and inserting these in the energy release rate of a straight long interface crack (Ref 21):

$$G(t) = \tau \frac{1 - \nu^2}{2(1 - \nu)^2} \int_y^{d_{TBC}} E(t,x)\left((T(x) - T_{crack})\,\alpha_{TBC} + (T_{crack} - T_{cool})\,(\alpha_{TBC} - \alpha_{sub})\right)^2 dx \quad \text{(Eq 9)}$$

where T_{crack} and T_{cool} are the temperatures at the crack location and during cooling, α_{TBC} and α_{sub} are the thermal expansion coefficients of TBC and substrate, the additional factor τ is described below. It should be mentioned that the considered stresses here are the in-plane stress states. The additional stress state closes to the interface according to Eq 2 are not taken into account as they are typically comparably low.

Failure will occur if the following condition holds:

$$G(t) \geq G_{crit} \quad \text{(Eq 10)}$$

The factor τ is added as the formula describes the energy release rate for a long ($c \gg d_{TBC}$) interface crack and high stress levels. For shorter cracks, the release rate is reduced. The crack length evaluated in the model are typically shorter ($< L$) than the TBC thickness. The argument is now, although in one direction the crack growth follows the described model, the cracks are two-dimensional objects which are interconnected (e.g., shown by the high gas permeability of the coatings) and by this giving increased efficient cracks lengths and significant energy release rates.

The factor τ was fitted by using the data for new TBC single-layer systems. These coatings typically spall-off at the interface without significant TGO growth due to the lower toughness of the TBC and hence the reduced critical energy release rate (10-20% of YSZ, corresponding to 15-30 J/m^2 (Ref 22), 30 J/m^2 is used). As mean time to spallation, we use 60 h at temperature (1050/1250 °C) which are about 500 standard cycles (Ref 23). With this value, a factor τ of 0.24 is obtained which is fixed for all calculations. A summary of the used model parameters is given in Table 1.

Table 1 The used model parameters

Amplitude A, μm	10/5, see text
Wavelength L, μm	50
Substrate thickness, mm	3
Bond coat thickness, mm	0.15
TBC thickness, mm	0.4
Young's modulus substrate, GPa	191
Poisson's ratio substrate	0.3
Thermal expansion coefficient substrate, 1/K	1.58×10^{-6}
Thermal conductivity substrate, W/m/K	26
Young's modulus bond coat, GPa	70
Poisson's ratio bond coat	0.43
Thermal expansion coefficient bond coat, 1/K	1.68×10^{-6}
Thermal conductivity bond coat, W/m/K	31.6
Young's modulus TGO, GPa	360
Poisson's ratio TGO	0.22
Thermal expansion coefficient TGO, 1/K	8×10^{-6}
Thermal conductivity TGO, W/m/K	7
Young's modulus TBC, GPa	20
Poisson's ratio TGO	0.33
Thermal expansion coefficient TBC, 1/K	1×10^{-6}
Thermal conductivity TBC, W/m/K	1.0
TGO growth coefficient A_{TGO}, m/s^p	7.48×10^{-4}
TGO growth activation energy, E_{TGO}, eV	0.907
TGO growth exponent	0.25
TBC sintering coefficient A_{sint}, s^m	2×10^{10}
TBC sintering activation energy E_{sint}, eV	3
TBC sintering exponent	0.25
TBC viscosity, Pa s	3.6×10^{14}
Fracture energy, J/m^2	150

The outlined model equations have been implemented into a Java program. The program reads input files in which the model parameters are stored. First, the fitting parameter is determined by using the known lifetime of a specific run. Subsequently, a rather unlimited number of different input parameter files can be read and the lifetime as well as other relevant data are calculated and stored in corresponding output files.

3. Experimental

Different types of TBC systems have been investigated. They were produced by atmospheric plasma spraying with an A3000 unit by Sulzer Metco (Wohlen, Switzerland) using a TRIPLEX I gun. Vacuum plasma spraying (VPS) with a F4 gun (Sulzer Metco, Wohlen, Switzerland) was used to deposit a 150-μm NiCoCrAlY BC (Ni 192-8 powder by Praxair Surface Technologies Inc., Indianapolis, IN) on disk-shaped nickel base IN738 superalloy substrates (diameter 30 mm, 3 mm thickness), which were used for thermal cycling experiments.

Details on the process conditions are given in Ref 24, 25), a summary of the coating characteristics is given in Table 2. As YSZ powder, a 7.8 wt.% yttria-stabilized

Table 2 Characteristics of the investigated APS coatings

Set	Thickness, µm	Porosity, %	HV0.1, GPa	*E**, GPa	Estimated mean thermal conductivity, W/m/K	Characteristics
S	400	12	6.3	163,142,104 **136-20**	1	Standard
SM	400	12	9.3	158,134,127 **140-21**	1	Higher microcrack density
ST	700	12			1	Thick
D	400	12 (?)	8.9	148,157,127 **144-21**	1.1	Lower porosity
P	400	15	7.0	128,138,110 **125-18**	0.9	Higher porosity
SE	450	8	4.1	185,207,185 **192-28**	1.4	Segmentation cracks, ~4, mm

*Young's modulus *E* at 10, 100, and 1000 mN and with mean value (*bold*) and extrapolated Young's modulus as described in the text

zirconia powder (Metco 204 NS) supplied by Sulzer Metco GmbH, Hattersheim, Germany, was used.

Besides the manufacture of the thermal cycling specimens, steel substrates were also coated. These coatings were used to characterize the as-sprayed condition. The porosity level was measured on free-standing coatings by mercury (Hg) porosimetry using two units of porosimeters produced by CE Instruments, Italy (Pascal 140 for the low pressure and Pascal 440 for the high pressure range). Coatings were removed from the substrates by using hydrochloric acid.

Stiffness values were determined by depth-sensing microindentation, details are given in Ref 26. For modeling, Young's moduli from bending tests seem to be more adequate. Values for the standard material of 20 GPa have been determined by this technique (Ref 27). This value was taken as a basis to calculate also the other values (see Table 1).

Thermal cycling was performed in one of our gas burner test facilities operating with natural gas and oxygen. The substrates were cooled by compressed air from the back. The surface temperature was measured with a pyrometer operating at a wavelength of 8-11.5 µm and a spot size of 12 mm. The emissivity of YSZ for this wavelength range was determined to be close to 1. Additionally, the substrate temperature was measured by a thermocouple mounted in a hole drilled toward the center of the substrate from one side. The surface temperature was adjusted close to 1250 °C, the substrate temperature was tried to be maintained as a mean value between 1050 and 1075 °C. Due to high thermal conductivity of the coatings and limited heat flux (<1 MW/m^2), this was not possible in all cases. Using the thermal conductivities of the coatings and the substrate, one can estimate that the BC temperature is about 20-40 K higher than the substrate temperature.

In the test facilities, gas burners with a broad flame are used giving a rather homogeneous temperature distribution in the center of the samples. After heating for less than a minute stationary conditions are obtained. After 5 min, the burner is automatically removed for 2 min from the surface and the surface is cooled from the front at an initial rate of more than 100 K/s using compressed air.

Cycling is stopped when a clearly visible spallation of the coating occurred. However, the specimens are not inspected after each cycle and the installed automatic system can only detect spallation if a rather large temperature change occurs at the surface of the coating. As a result, a certain number of cycles can be performed even after spallation which gives a certain uncertainty in the number of cycles typically below 20% of the total cycle count.

In addition to this cyclic burner tests, furnace tests have also been performed. The specimens were kept in a furnace for 24 h at 1100 °C under air atmosphere and removed afterward for 1 h. During this time, the samples cooled down to room temperature at moderate cooling rates. During weekends the samples remained in the furnace giving longer dwells times.

Metallographic cross sections have been prepared from all samples to investigate the microstructure. The coatings have been imbedded in epoxy before cutting to reduce the possibility of damage.

For the TGO thickness investigation, a scanning electron microscope (Phenom, FEI) was used. About 50 measurements per data point have been taken. The depleted zone was measured with an optical microscope.

4. Experimental Results and First Discussion

4.1 Lifetime Data

The results of the burner rig testing are shown in Fig. 3. Time to failure is the hot time assuming 5 min per 5/2 min cycle. For each type of coating, two samples have been tested. Obviously, the number of cycles to failure are decreasing with increasing BC temperatures. In addition, the two samples of one type of coating show very similar results if the general dependence on the BC temperature (indicated by the straight line) is considered. These results allow some kind of ranking of the microstructures: the best TBCs are those with porous and modified structures, the others as standard, dense, thick standard, and segmented appear within the scatter range quite similar.

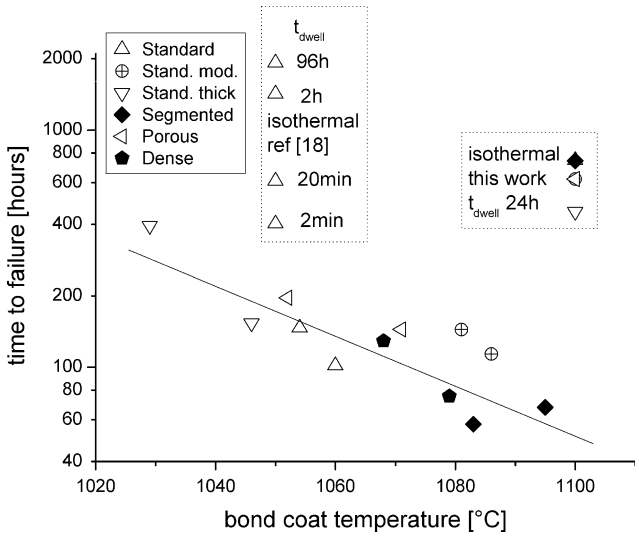

Fig. 3 Cycles to failure in our burner rigs for the different systems as a function of BC temperature. In addition, results for isothermal tests are plotted: furnace testing at 1100 °C in our institute (approximately 1 day cycles including 1 h cooling) and results obtained with our standard system from reference (dwell time at 1050 °C given, 1 min at 60 °C, cylindrical samples with 8.5 mm diameter; Ref 13)

One should add here that the tested segmented coating was one with a segmentation crack density of about 4/mm. Meanwhile process improvement led to coatings with much higher densities of more than 10/mm.

In addition, also results from furnace tests at 1100 °C and literature results in which our coatings were used (Ref 13) are given. It should be mentioned that the samples used in Ref 13 are cylindrical samples with diameter of 8.5 mm with substrates made of CMSX4. In the modeling, we will ignore this fact and assume flat IN738 substrates for all calculations.

In Fig. 4, photos of one of each type of sample are shown after failure. Also two furnace test samples are included. They show a total spallation of the TBC.

4.2 Microstructure and TGO Growth

In Fig. 5, the TGO thickness at failure in the center of the samples is plotted for the different samples. With this measurement information on the influence of the microstructure on the failure should be obtained. The idea was that a better/improved microstructure should give a higher TGO thickness at failure. In contrast to the expectations only some differences in the TGO thickness values are found. For example, the segmented coatings show relatively low thickness values. In Fig. 6(a-f), the microstructures of the TBCs close to the BC/TBC interface are shown. Especially in the burner rig tests, the samples show cracks running in the TBC close to the TBC/BC interface at a distance close to the one chosen in the model (20 μm). The examples in Fig. 6 show that especially in areas with high modulations rather thick TGOs are found because the TGO layers of the two parts of a hill location grow together. In order to take into account this local overestimation of the TGO thickness, the maximum 20% of the data have been excluded. This procedure reduced the scatter of the data considerably, however, still no distinct correlation between microstructure and TGO thickness at failure was found. Certainly, also the tendency of the used BC to form large areas of internal oxidation leads to additional problems in a precise determination of the TGO thickness. In Fig. 7, the TGO thickness values for both types of evaluation are shown. Obviously, the TGO thickness at failure is reduced with increasing BC temperature. According to Eq 3, a plot of the TGO thickness divided by the number of cycles with an exponent of 0.33 is shown. This should follow an Arrhenius-type behavior, i.e., an increase with temperature is expected. In contrast, the data points indicate more likely a decrease. Looking on the thickness of the depleted zone, a rather large scatter is observed. Despite of this scatter, a reduction of thickness with increasing BC temperature is not observed. The thickness of the depleted zone divided by the cycle number with an exponent of 0.33 shows in the middle an increase with temperature. These results can be explained by a change of TGO morphology with changing temperature, i.e., the TGO becomes denser or shows a lower amount of internal oxidation with increasing temperature. This can explain why the TGO thickness decreases while the depleted zone correlated to the amount of consumed aluminum increases with rising temperature. The different micrographs in Fig. 6 in the order of increasing BC temperature seem to be consistent with this hypothesis. On the other hand, this hypothesis is not included in our model, in which a simple thermally activated growth of the TGO is assumed. To keep the model simple, we use an ordinary growth law as given for our BC in Ref 13. With this kinetics the high-temperature values fit to our experimental data for the TGO thickness (i.e., 50 h at 1100 °C correspond to about 7 μm TGO thickness). Our assumption for the lower temperature is that the large internal oxidation and the mixed oxide formation of this BC correlates in fact to a lower effective TGO thickness with respect to stress build-up at the interface. At higher temperature, the enhanced selective oxidation of aluminum leads then to a pure alumina scale.

5. Comparison of Experimental and Modeling Results

The results shown in Fig. 3 indicate that the lifetime of a TBC system is extremely depending on the given operation or test conditions. Although the lifetime model was mainly developed to describe the lifetime data of samples tested in our burner rigs (the lower values in Fig. 3), it should also be able to account for additional influencing factors as cycle length or the temperature profile during testing (gradient or isothermal). In addition, the generally found temperature dependence should also be predicted in an adequate way. As another important feature, the model should be able to describe in at least a

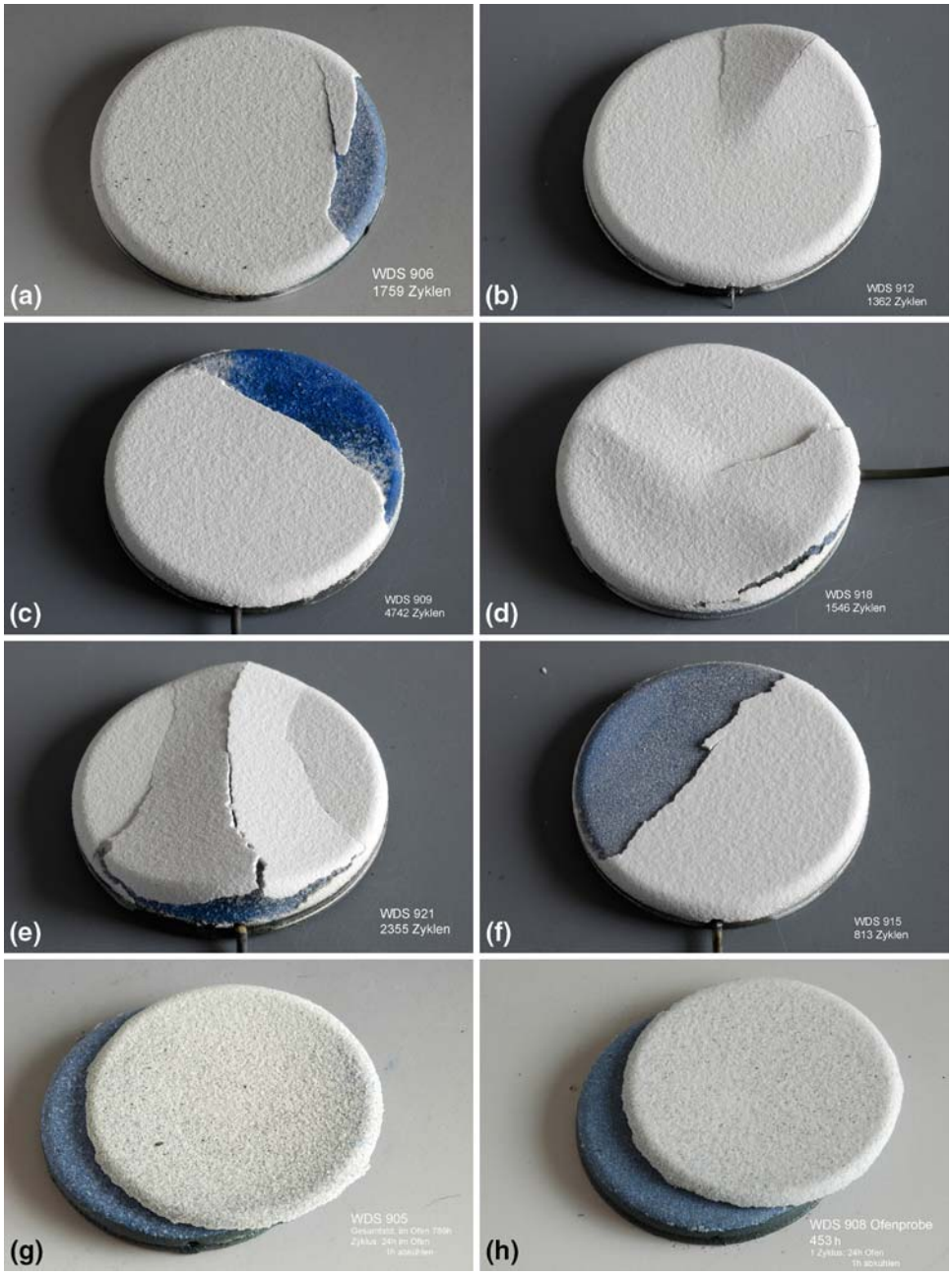

Fig. 4 (a-e) Photos of the samples after failure, rig-tested samples in the order according to Table 2 for sample a to f. Photos (g) and (h) correspond to standard and the thick coatings after the furnace tests

semi-quantitative way the influence of the microstructure of the TBCs on their performance.

5.1 Influence of the Data Used for Fitting on Modeling Results

The first step in applying the model is the determination of the fitting factor $A^*(Y/K_{Ic})^m$ describing the crack growth behavior and given in Eq 5. Doing that it turns out that the results of the calculations are rather largely depending on the used starting value for fitting. If a data point with a long lifetime (e.g., in Fig. 3 > 1000 h at 1050 °C) is taken, the cycle length dependence for the isothermal cycling could be reproduced quite nicely; however, the predicted lifetime of the rig samples is very long. On the other hand, if the burner rig data are used for fitting, the predicted lifetime of isothermal experiments are typically too short. It indicates that for the given parameters and input data, the model does not precisely describe the cycle dependence of the lifetime data. On the other hand, it should be stated that no optimization loops for the model parameters have been used and certainly

several of the parameters are rather uncertain as pointed out below. In addition, it also should be mentioned that the investigated range of test conditions is extremely wide, so a detailed description by a single model is anyhow ambitious.

Finally, it was decided to use as fitting data the isothermal data from literature (Ref 13) with a short dwell time (20 min at 1050 °C). For these parameters, we obtain a fitting factor of 10^{-97} m/s (Pa $m^{1/2})^{-m}$ which appears rather large compared to expectations from literature

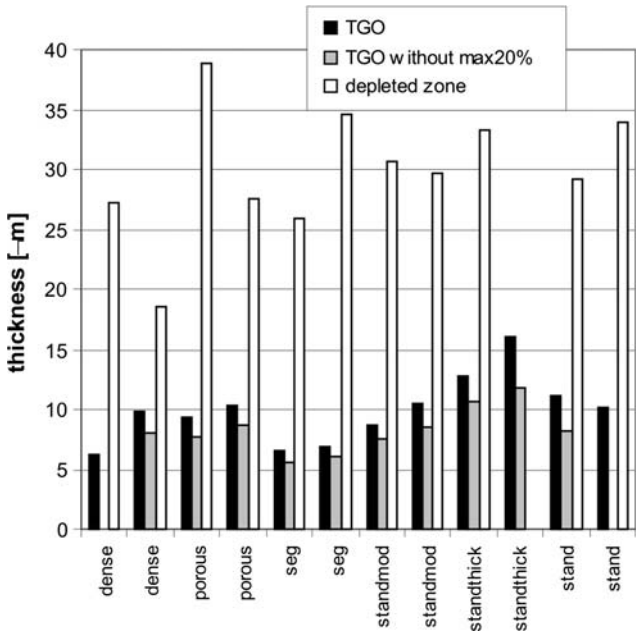

Fig. 5 Thickness of TGO and depleted zone of rig samples for the different types of samples

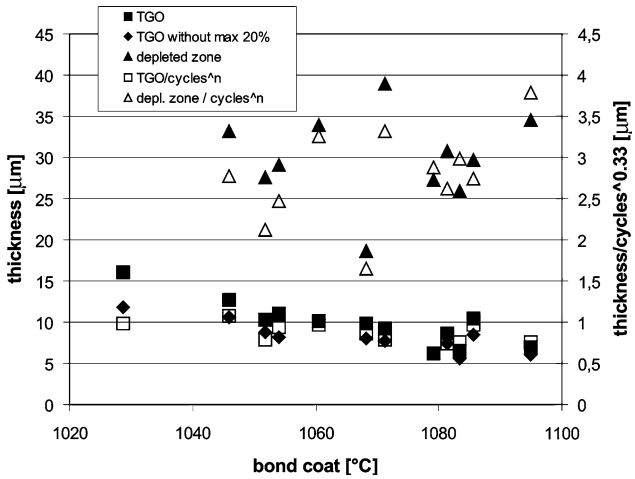

Fig. 7 Thickness of TGO and depleted zone of the rig samples as function of the BC temperature (*filled symbols*). In addition the thickness values divided by the cycle number with an exponent of 0.33 are given (*open symbols*)

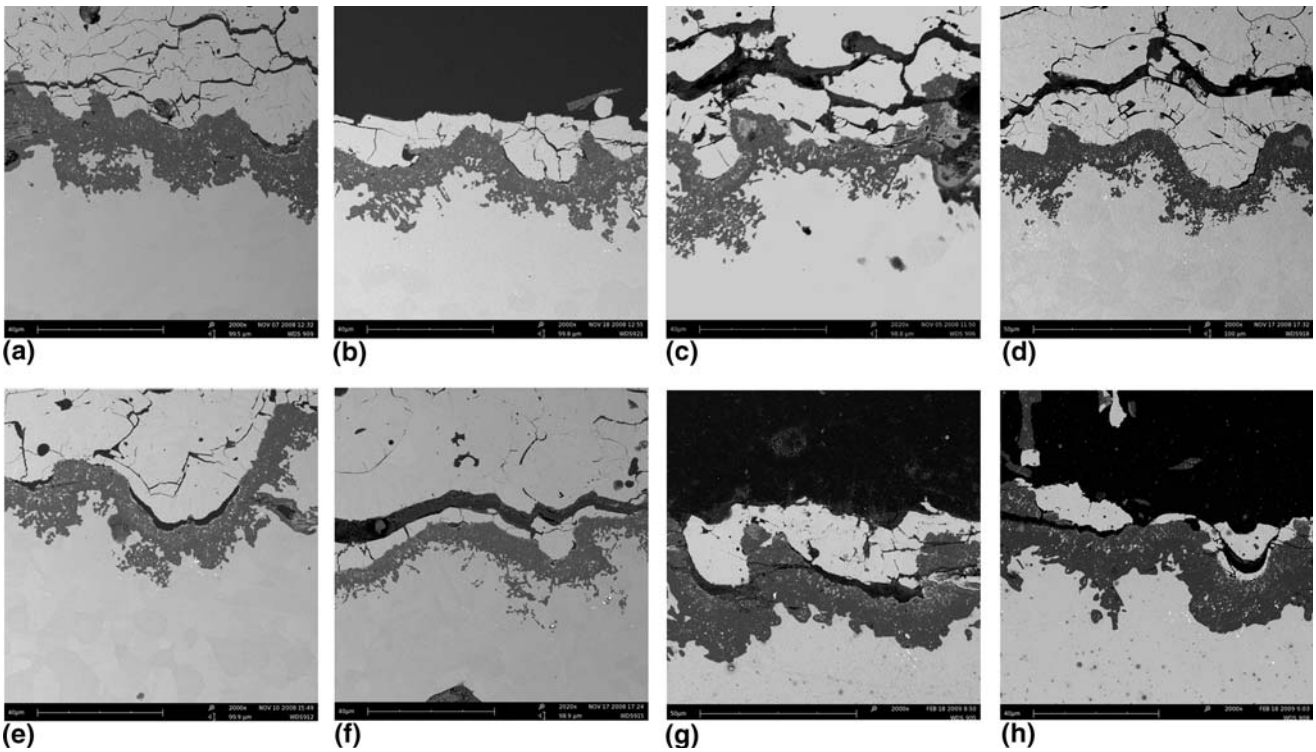

Fig. 6 SEM micrographs of failed rig samples at the BC TBC interface ((a) to (f) order according to Table 2 with increasing temperature, (g) and (h) correspond to furnace tests at 1100 °C, see also text)

data (Ref 17). On the other hand, the uncertainty in the stress determination at the interface and the uncertainty of all experimental data (e.g., taking a Young's modulus of 40 GPa used in Ref 17 instead of 20 GPa reduces the factor by more than five orders of magnitude) might explain this deviation.

In Fig. 8(a), a comparison between the experimental data given in Fig. 3 and our modeling results are shown. Obviously, the temperature dependence of the lifetime can be predicted; however, the actual lifetime of the burner rig samples is by a factor of 3 to low. The temperature dependence reflects the temperature dependence of the TGO growth rate. This indicates that the approximation for the growth kinetics discussed above is adequate.

A better fit can be obtained by using one of the burner rig data points for fitting. The result is that the fitting factor (the crack growth constant) becomes very large, which appears not really physical meaningful. Simultaneously, all data points for one temperature tend to lie close together. Once the critical TGO thickness for stress inversion is reached, fast crack growth sets in leading to failure close to this time.

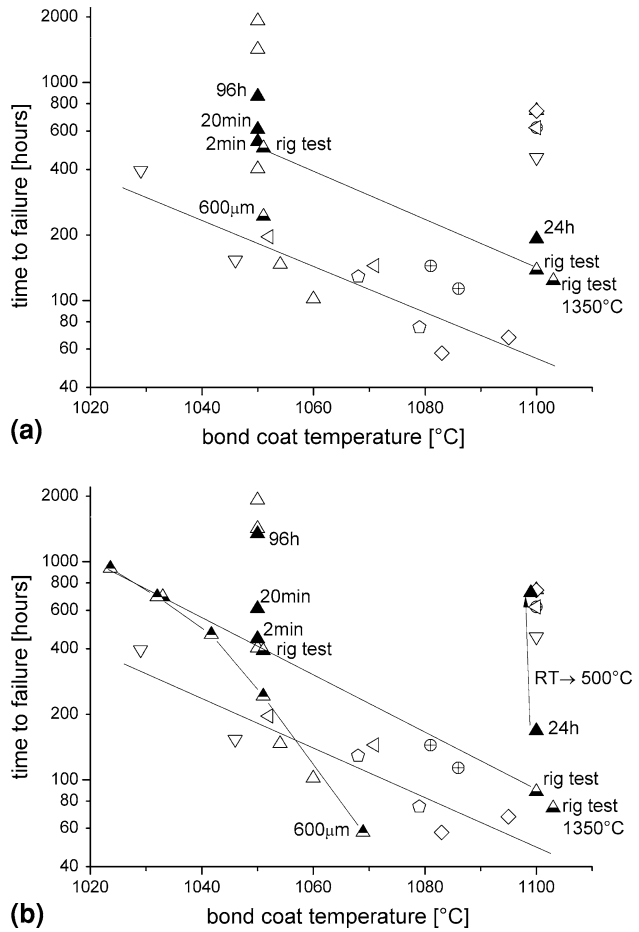

Fig. 8 Comparison of experimental (see Fig. 3) and modeling results: (a) amplitude 10 µm, (b) amplitude 5 µm. *Open symbols*: experimental results, filled and half-filled symbols: modeling results of furnace and burner rig tests, respectively. In (b) also a number of modeling results for a 600-µm thick coating are included

5.2 Influence of the Analytical Stress Approximation on Modeling Results

One additional feature of the model which has to be optimized is the analytical description of the stress state close to the TGO in the TBC. Figure 9 shows the development of the stress state with TGO thickness. Obviously, it exists a rather steep increase of the stress levels after reaching the critical TGO thickness for stress inversion for the amplitude of 10 µm. The slope of this curve largely influences the crack growth kinetics as the stress enters with a high exponent ($m = 18$, see Eq 5) in the crack growth law. An improved accuracy might be possible from more detailed FE calculations for the given interface morphology instead of using a general formula as done here. However, this makes the model rather inflexible. Being aware that the analytical stress function is critical for the outcome of the lifetime model, it is tried to modify this by using a different roughness value (amplitude A). Additionally, as for several other parameters used in the model, the given value of 10 µm is only a mean value and therefore a simplifying approximation of a complex structure. The stress evolution for an amplitude of 5 µm is also shown in Fig. 9. It clearly shows a smoother increase with increasing TGO thickness.

The results obtained for an amplitude of 5 µm are shown in Fig. 8(b). Obviously, the modeling results are much closer to the experimental results, especially to the furnace tests at 1050 °C. Also, the fitting factor $A^*(Y/K_{Ic})^m$ appears to be more reasonable (4.2×100^{-102} m/s $(\text{Pa}^*m^{1/2})^{-m}$). In addition, the burner rig lifetimes obtained by the model are reduced and by that closer to the experimental results. The remaining deviation seems to indicate that the thermal cycling in our burner rigs generates additional stress levels not

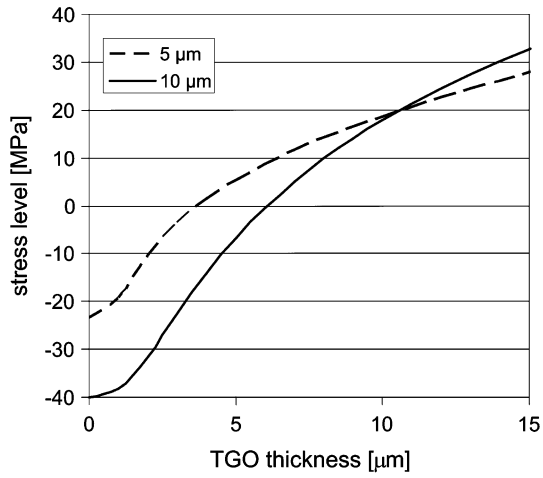

Fig. 9 Stress levels in the TBC developed at a distance of 20 µm from the valley locations for the used interface roughness ($A = 5 + 10$ µm, $L = 50$ µm) as a function of TGO thickness

included in the model which further promote crack growth. One possibility which is already included in the model is the thermal gradient itself. The gradient will lead to a faster increase of the Young's modulus close to the surface and by this also to a faster increase of the strain energy of the coating. On the other hand, the higher surface temperature and by that the large contraction of surface near regions during cooling will reduce the mismatch strain and by this the critical energy release rate (see Eq 9). We tried in the results shown in Fig. 8a) to stress the effect of the sintering compared to the expansion effect by choosing a relatively high activation energy for sintering (3 eV), which still fits experimental data reasonably. Sintering seems just to compensate the expansion effect.

An additional influencing parameter might be the transients in thermal cycling. In the burner rig tests, we apply cooling of the TBC surface by compressed air leading to a distinct stress inversion in the coatings. An approximate calculation shows that the developed strain energies can be close to the critical energy release rate after some sintering (~100 J/m^2). Hence, in a future model this additional driving force has to be included.

Also shown in Fig. 8(b) is the effect of the surface temperature by increasing it from 1250 to 1350 °C. Lifetime is reduced from 93 to 74 h for rather constant BC temperature of 1100 °C. This can be explained by the enhanced sintering.

The results for the furnace testing at 1100 °C is still lower than the experimental findings. Here it is also tried to take into account the more enhanced relaxation due to slow cooling for the furnace testing at 1100 °C by introducing a relatively high lower temperature level (500 °C instead of RT). With this, the experimental results can be fitted very nicely.

Figure 8(b) also shows modeling results for thicker TBCs (600 μm instead of 400 μm as standard). While for BC temperatures below about 1040 °C, the results are similar to those of thinner coatings a reduction is found for higher temperatures. The higher slope in the logarithmic lifetime versus inverse temperature plot indicates a dominating process with a higher activation energy. The modeling results show that no crack growth occurs at higher temperatures in the thick TBCs. Only the strain energy build-up by sintering leads to the failure. As we use sintering with a rather high activation energy, the slope of the corresponding curve becomes rather steep. These results might explain why the lifetime of the thick coating at low temperatures was so high while at higher temperatures the lifetime drops considerably (see inverse triangles in Fig. 8b).

5.3 Influence of Microstructural Variations on Modeling Results

Figure 10 shows the influence of Young's modulus on the lifetime according to our model. Here different *E*-moduli are used as given in Table 1. Obviously, also a rather low increase of the Young's modulus reduces lifetime considerably. The improvement of the lifetime for

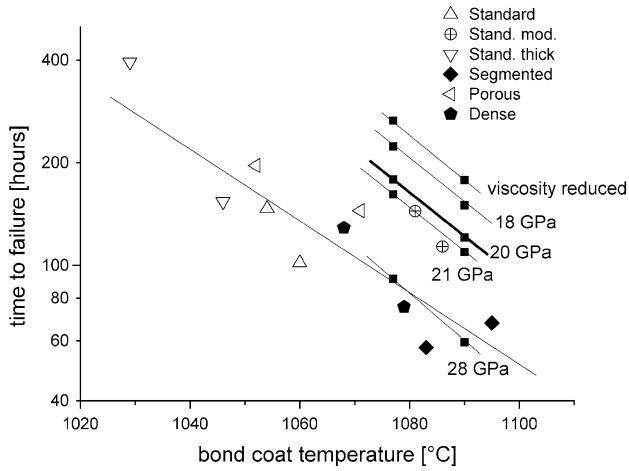

Fig. 10 Lifetime of the burner rig samples compared to modeling results for samples with different microstructure/Young's moduli at two temperatures (1077 and 1090 °C). The symbols connected with the *bold line* indicate the reference (20 GPa). In addition, results for reduced viscosity values (100 times reduction) are included

the porous coating seems to be reproduced by the modeling result (compare 20 and 18 GPa). The reduction of lifetime for the segmented coating with the high Young's modulus slightly overestimates the effect. This might be explained by the different stress state developed in such segmented coatings. The segmentation cracks should reduce stress levels and by that overcompensate the detrimental effect of the increased Young's modulus. This seems to be not fully possible by the tested segmented coatings. However, as mentioned before, new segmented coatings with higher crack densities show improved thermal cycling performance.

Interesting is also the good performance of the so-called modified standard TBC. By using a higher number of passages more microcracks are introduced into the coating. This can lead to a more pronounced stress relaxation which we try to model by a reduced viscosity in the coating. Indeed, a rather large reduction of viscosity by a factor of 100 can explain the good thermal cycling results of our modified coatings.

The influence of relaxation (see Eq 7) for the standard viscosity value will finally be briefly discussed. The experimental value for the viscosity gives a significant relaxation at low temperature only for times in the order of hours. Hence, for most of the given experimental results, the effect is rather negligible. Only for the furnace testing at 1100 °C, a significant increase of the lifetime is observed due to the introduction of the relaxation. Of course, for longer dwell times at low temperatures (or lower viscosity coatings) this effect becomes more relevant.

6. Summary

A lifetime model for TBCs was presented which combines the influence of several features as TGO growth, BC

roughness profile, sintering within the ceramic, Young's modulus and thickness of the ceramic, thermal gradients and the precise shape of the applied thermal cycles. This was possible by combining a crack growth with an energy release rate based model.

The outcome of this model was compared to the results of a number of different burner rig and cyclic oxidation experiments. By an adjustment of the amplitude of the roughness profile it was possible to reproduce the experimental findings in a very satisfying way. Only the burner rig tests showed somewhat lower lifetimes which was attributed to additional transient stress buildup which was not yet implemented in the model.

Also, the influence of different types of TBCs with varying porosity, microcrack density and coating thickness on the lifetime results could be at least qualitatively explained by the model results.

Acknowledgments

The support of Dr. Franziska Träger and especially of Dr. Jose Marques for performing Ansys calculations of the stress state and developing an analytical formula to describe the results are gratefully acknowledged. Special thanks to Dr. Jürgen Malzbender, IEF-2, Forschungszentrum Jülich GmbH, for performing the indentation tests for the determination of Young's moduli. The authors also gratefully acknowledge the work of Mrs. Sigrid Schwartz-Lückge for carrying out scanning electron microscopy, of Mr. Karl-Heinz Rauwald, Mr. Frank Vondahlen, and Mr. Ralf Laufs for the manufacturing of the TBC systems, and of Mrs. Dr. Doris Sebold for SEM work and fruitful discussion on the oxidation test results. Also many thanks to Mrs. Nicole Hilgers for the thermal cycling work. The presented results have partly been made within a German research project MARCKO—thermal barrier coating systems, financed by the German Federal Ministry of Economics and Technology.

References

1. Y.C. Zhou and T. Hashida, Thermal Fatigue Failure Induced by Delamination in Thermal Barrier Coating, *Int. J. Fatigue*, 2002, **24**(2-4), p 407
2. A.M. Freborg, B.L. Ferguson, W.J. Brindley, and G.J. Petrus, Modelling Oxidation Induced Stresses in Thermal Barrier Coatings, *Mater. Sci. Eng. A*, 1998, **245**, p 182
3. M.Y. He, A.G. Evans, and J.W. Hutchinson, The Ratcheting of Compressed Thermally Grown Thin Films on Ductile Substrates, *Acta Mater.*, 2000, **48**, p 2593
4. A.M. Karlsson and A.G. Evans, A Numerical Model For the Cyclic Instabilities of Thermally Grown Oxides in Thermal Barrier Coating Systems, *Acta Mater.*, 2001, **49**, p 1793
5. R. Vaßen, G. Kerkhoff, M. Ahrens, and D. Stöver, *Life Time Prediction Model for Plasma-Sprayed Thermal Barrier Coatings Based on a Micromechanical Approach*, Ceramic Materials and Components for Engines, J.G. Heinrich and F. Aldinger, Ed., Wiley, VCH, Weinheim, 2001, p 182
6. R. Vaßen, G. Kerkhoff, and D. Stöver, Development of a Micromechanical Life Prediction Model for Plasma Sprayed Thermal Barrier Coatings, *Mater. Sci. Eng. A*, 2001, **303**(1-2), p 100-109
7. G.C. Chang, W. Pucharoen, and R.A. Miller, Finite Element Thermal Stress Solutions for Thermal Barrier Coatings, *Surf. Coat. Technol.*, 1987, **30**, p 13
8. R.A. Miller, Oxidation-Based Model for Thermal Barrier Coating Life, *J. Am. Ceram. Soc.*, 1984, **67**, p 517
9. J.T. DeMasi, K.D. Sheffler, and M. Ortitz, ''Thermal Barrier Coating Life Time Prediction Model Development, Phase 1 Final Report,'' NASA Report, vol. CR182230, 1989
10. M. Oechsner,''Ein Beitrag zur Lebensdauervorhersage von keramischen Wärmedämm-schichten,'' VDI Fortschrittsberichte, 263, 2001
11. D. Renusch, H. Echsler, and M. Schütze, Progress in life time modelling of APS-TBC Part I: critical strains, macro-cracking, and thermal fatigue, *Mater. High Temp.*, 2004, **21**, p 65-76
12. D. Renusch, H. Echsler, and M. Schütze, Progress in Life Time Modelling of APS-TBC, Part II: Critical Strains, Macro-Cracking, and Thermal Fatigue, *Mater. High Temp.*, 2004, **21**(2), p 77-86
13. O. Trunova, T. Beck, R. Herzog, R.W. Steinbrech, and L. Singheiser, Damage Mechanisms and Lifetime Behavior of Plasma Sprayed Thermal Barrier Coating Systems for Gas Turbines—Part I: Experiments, *Surf. Coat. Technol.*, 2008, **202**, p 5027-5032
14. T. Beck, R. Herzog, O. Trunova, M. Offermann, R.W. Steinbrech, and L. Singheiser, Damage Mechanisms and Lifetime Behaviour of Plasma-Sprayed Thermal Barrier Coating Systems for Gas Turbines—Part II: Modelling, *Surf. Coat. Technol.*, 2008, **202**, p 5901-5908
15. E.P. Busso, H.E. Evans, L. Wright, L.N. McCartney, J. Numm, and S. Osgerby, A Software Tool for Lifetime Prediction of Thermal Barrier Coating Systems, *Mater. Corros.*, 2008, **59**(7), p 556-565
16. M. Ahrens, R. Vaßen, and D. Stöver, Stress Distributions in Plasma-Sprayed Thermal Barrier Coatings as a Function of Interface Roughness and Oxide Scale Thickness, *Surf. Coat. Technol.*, 2002, **161**, p 26-35
17. F. Traeger, M. Ahrens, R. Vaßen, and D. Stöver, A Life Time Model for Ceramic Thermal Barrier Coatings, *Mater. Sci. Eng.*, 2003, **A358**, p 255-265
18. M. Ahrens, S. Lampenscherf, R. Vaßen, and D. Stöver, Sintering and Creep Processes in Plasma-Sprayed Thermal Barrier Coatings, *J. Therm. Spray Technol.*, 2004, **13**(3), p 432-442
19. D. Munz and T. Fett, *Ceramics Springer Series in Materials Science*, Springer-Verlag, Berlin, 1999
20. T. Patterson, A. Leon, B. Jayaraj, J. Liu, and Y.H. Sohn, Thermal Cyclic Lifetime and Oxidation Behavior of Air Plasma Sprayed CoNiCrAlY Bond Coats for Thermal Barrier Coatings, *Surf. Coat. Technol.*, 2008, **203**, p 437-441
21. G.P. Cherepanov, *Mechanics of Brittle Fracture*, McGraw-Hill, New York, 1979, p 640
22. U. Bast and E. Schumann, Development of Novel Oxide Materials for TBCs, *Ceram. Eng. Sci. Proc.*, 2002, **23**(4), p 525-532
23. R. Vaßen, F. Traeger, and D. Stöver, New Thermal Barrier Coatings Based on Pyrochlore/YSZ Double-Layer Systems, *Int. J. Appl. Ceram. Technol.*, 2004, **1**(4), p 351-361
24. R. Vaßen and D. Stöver, *Influence of Microstructure on the Thermal Cycling Performance of Thermal Barrier Coatings*, Thermal Spray 2007: Global Coating Solutions, Beijing, PR China, B.R. Marple, M.M. Hyland, Y.-C. Lau, C.-J. Li, R.S. Lima, and G. Montavon, Ed., 14-16 May 2007, ASM International, Materials Park, OH, USA, 2007
25. R. Vaßen, H. Guo, and D. Stöver, *Manufacture and Properties of Segmented Thermal Barrier Coatings*, Proceedings of the 29th Int. Cocoa Beach Conf. & Exposition, Cocoa Beach, Fl., D. Zhu and W.M. Kriven, Ed., 23-28 Jan, *Ceram. Eng. Sci. Proc.*, **26**(38), 2005, p 37-45
26. J. Malzbender and R.W. Steinbrech, Determination of Stress-Dependent Stiffness of Plasma-Sprayed Thermal Barrier Coatings Using Depth-Sensitive Indentation, *J. Mater. Res.*, 2003, **18**(8), p 1975-1984
27. T. Wakui, J. Malzbender, and R.W. Steinbrech, Stress Analysis of Plasma Sprayed Thermal Barrier Coatings and Mechanical Stress, *J. Therm. Spray Technol.*, 2004, **13**(3), p 390-395